CrossMark

RESEARCH

Molecular dynamics and density functional theory study on the corrosion inhibition of austenitic stainless steel in hydrochloric acid by two pyrimidine compounds

Fahimeh Shojaie[1] · Nasser Mirzai-Baghini[2]

Abstract Quantum chemical calculations based on density functional theory method were performed on two pyrimidine derivatives which may be used as corrosion inhibitors for austenitic stainless steel. The quantum chemical properties of the two pyrimidine derivatives that are most relevant to their potential action as corrosion inhibitors have been calculated. To explain the inhibition performance of the pyrimidine derivatives, their local reactivities were analyzed through Fukui functions. The binding energies of the inhibitors with the surface of austenitic stainless steels were studied. A model has been suggested to calculate the approximate inhibition efficiencies of the pyrimidine derivatives. All calculations were carried out in both gas and liquid phases.

Keywords Quantum chemical descriptors · Corrosion inhibitors · Density functional theory (DFT) · Austenitic stainless steel · Quantitative structure and activity relationship (QSAR) · Molecular dynamics simulation

Introduction

Austenitic stainless steels are iron–chromium–nickel (Fe–Cr–Ni) alloys. They may contain small amounts of other alloying elements, e.g., Mn, Nb, Mo, Si, Al and Ti, which

may alter their specific properties. The formation of a passive layer of corrosion inhibitors on surfaces of these materials causes high corrosion resistance [1, 2]. Because of their strength, corrosion resistance, mechanical workability, and excellent electrical and thermal conductivities, austenitic stainless steels are one of the most important materials that are used widely in different industries [3–6]. The corrosion of stainless steel, especially when it occurs in acidic solution, is the concern of the steel users [7]. Acidic solutions are the cause of the detriment to many materials and considerable economic losses [8–10].

The corrosion inhibition efficiency depends on the structure, chemical composition, the nature of the metal and other conditions [11]. Theoretical studies of the efficiency of corrosion inhibitors have aimed at gaining insight on the molecular chemical activity, structural and electronic properties [12–17]. Newly, experimental and quantum chemical studies on inhibition of the corrosion of steel by two pyrazole compounds [18], benzothiazole derivatives [19], 1H-pyrrole-2,5-dione derivatives [20], some sulfonamides [21] and Schiff base molecules [22] have been calculated. The density functional theory calculations were performed on benzoin, benzil, benzoin-(4-phenylthiosemicarbazone) and benzil-(4-phenylthiosemicarbazone) used as corrosion inhibitors for mild steel in acidic medium by Kayadibi et al. [23]. The effect of temperature on corrosion and inhibition processes is discussed by Odozi et al. [24]. They showed that corrosion rate increases as temperature increases both in the absence and presence of the inhibitor and decreases further in the presence of the inhibitor. Radilla et al. [25] have studied the adsorption of the corrosion inhibitor 2-mercaptoimidazole onto Fe (1 0 0) surface.

The presence of heteroatoms with a number of lone pairs of electrons may result in the protonation of the inhibitor at

✉ Fahimeh Shojaie
f.shojaie@kgut.ac.ir

[1] Department of Photonic, Institute of Science and High Technology and Environmental Sciences, Graduate University of Advanced Technology, Kerman, Iran

[2] Imperial College Reactor Centre, Silwood Park, Ascot, Berkshire, UK

Springer

the heteroatom centers. Therefore, several works have been done in this area. In the quinoline derivatives [26] (the N atom is the only heteroatom), protonated species is more electron deficient than the non-protonated species. Theoretical studies on phenazine and related compounds as corrosion inhibitors for mild steel in sulfuric acid medium [27] show that molecules with N atoms are preferentially protonated in acidic medium while molecules with S and O atoms do not prefer to undergo protonation, which confirms the results obtained from the calculation of the proton affinity. All the quinoxaline molecules have N atoms; they are all likely to be protonated in aqueous acid medium [28]. A comparison of the quantum chemical reactivity parameters for protonated species and the neutral species indicates the relative tendency of these species to interact with the metal surface.

The objective of this paper is to carry out a theoretical study on the corrosion inhibition effect of two pyrimidine derivatives, which have a class of sulfur and nitrogen-containing compounds. Caliskan et al. studied the corrosion inhibition effect of same pyrimidine derivatives in 1 M HCl solution at 298 K using polarization and impedance techniques [29]. The pyrimidine derivatives that were studied by us and also investigated by Caliskan et al. in their work are 5-Benzoyl-4-(4-carboxyphenyl)-6-phenyl-1,2,3,4-tetrahydro-2-iminopyrimidine (BCPTI) and 5-Benzoyl-4-tolyl-6-phenyl-1,2,3,4-tetrahydro-2-thioxopyrimidine (BTPTT) [29]. The composition of the studied austenitic chromium–nickel steel is as follows: (composition is expressed in weight %) C: 0.0425; Si: 0.421; Mn: 2.13; P: 0.0133; S: 0.113; Cr: 18.51; Mo: 0.563; Ni: 8.34; Al: 0.0334; Co: 0.0901; Cu: 0.358; Fe: balance [29].

Computational methods

The calculations on BCPTI and BTPTT were performed by Gaussian09 [30] software using the B3LYP function and the 6-311++G (d, p) basis set. This software has been used specifically for systems containing transition metal atoms. These calculations were performed to investigate the structural parameters that affect the inhibition efficiency of the two pyrimidine derivatives and also to study the adsorption mechanisms on the austenitic stainless steel surface. From the optimized geometries of BCPTI and BTPTT, their global molecular descriptors [31–44] such as the energy of the highest occupied molecular orbital (E_{HOMO}), the energy of the lowest unoccupied molecular orbital (E_{LUMO}), the energy gap (ΔE), the ionization potential (IP), the electron affinity (EA), the global hardness (η), the electronegativity (χ), the global softness (σ), the electrophilicity (ω), the electrodonating (ω^-), the

electroaccepting (ω^+), the net electrophilicity ($\Delta\omega^\pm$), the fraction of electron transferred (ΔN), the total negative charge (TNC) and the dipole moment (μ) were calculated. It is expected that the properties of molecules and ions to be different in gas and liquid phases. In this work, all calculations for solvent effect on the inhibitors were carried out using the IEFPCM method [45]. The theoretical results can be used to identify compounds with desired properties using quantitative structure activity relationship (QSAR) method [46]. The correlation between the inhibition efficiencies of the compounds indicated that QSAR method could be used to study the inhibitors. A quadratic model has been suggested to calculate the approximate inhibition efficiencies. According to this model, the regression analyses fitted the Caliskan et al. experimental data [29] well and the calculated inhibition efficiencies of the two pyrimidine derivatives were found to be close to their experimental values.

Results and discussion

Reactivity parameters

The structures and the optimized configurations of the BCPTI and PTPTT corrosion inhibitors are shown in Fig. 1. The inhibitor conformers are considered to be minima based on the absence of imaginary frequencies. The HOMO and the LUMO of the BCPTI and PTPTT inhibitors in gas and liquid phases are shown in Fig. 2.

The HOMO of the BCPTI molecule is delocalized throughout the system except on ring d and has maxima on C2, C6, C4, C8 and C10 atoms in particular on heteroatoms N and N2. The LUMO is delocalized throughout the BCPTI system except on ring a, and has maxima on ring d (see Fig. 2), C12 and O atoms in both gas and liquid phases. The HOMO of the BTPTT molecule is delocalized on ring b and has maxima on S and C12 atoms in gas phase. The maxima of the HOMO is delocalized on ring a, a slight delocalization on rings b and c and has maxima on S and C12 atoms. The LUMO is delocalized throughout the BTPTT system except on ring a in both phases (see Fig. 2). The LUMO of the BTPTT has maxima on C12 and C10 atoms in particular on heteroatoms O and S in both phases. The regions of a molecule on which their HOMO are distributed indicate the sites which have the highest tendency to interact with a metal surface. The LUMO indicates regions which have the highest tendency to accept electrons.

Table 1 shows the bond lengths and angles of the BCPTI and BTPTT inhibitors that are considered to be significant. A comparison of bond lengths and angles for both gas and liquid phases shows the effect of solvent on

Fig. 1 The structures and the optimized geometries of the BCPTI and PTPTT inhibitors
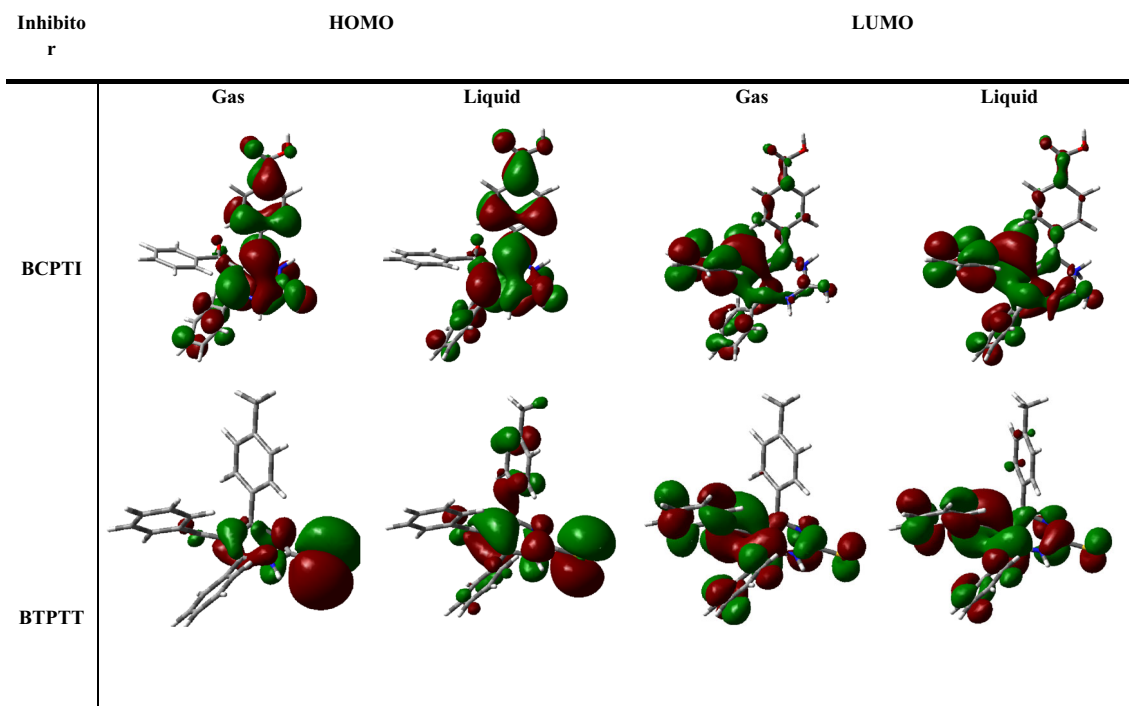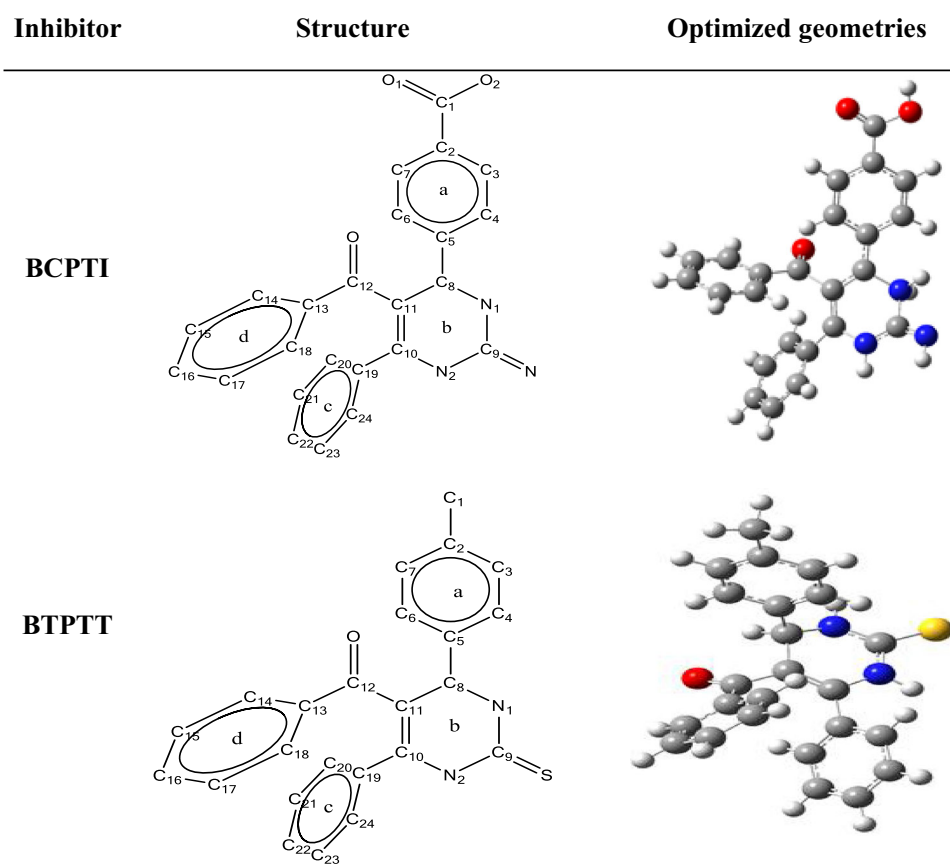

Fig. 2 The HOMO and the LUMO of the BCPTI and BTPTT inhibitors in gas and liquid

Table 1 Comparison of the bond lengths and bond angles of BCPTI and BTPTT in gas and liquid phases

	BCPTI		BTPTT	
	Gas	Solvent	Gas	Solvent
Bond lengths (Å)				
C1–O1	1.214	1.225	–	–
C1–O2	1.367	1.364	–	–
C1–C2	1.469	1.457	1.509	1.509
C2–C3	1.400	1.408	1.400	1.403
C3–C4	1.385	1.380	1.392	1.391
C5–C6	1.422	1.431	1.397	1.395
C2–C7	1.407	1.412	1.394	1.396
C5–C8	1.430	1.416	1.529	1.527
C9–N1	1.490	1.487	1.347	1.337
C9–S	–	–	1.675	1.695
C9–N	1.274	1.271	–	–
C9–N2	1.349	1.354	1.377	1.368
C10–C11	1.379	1.376	1.353	1.353
C12–O	1.217	1.225	1.225	1.229
C10–N2	1.428	1.418	1.400	1.402
Bond angles (°)				
O1–C1–O2	121.016	120.390	–	–
C1–C2–C3	120.827	122.922	120.976	120.788
C4–C5–C6	116.099	115.512	118.476	118.499
C1–C2–C7	119.047	119.611	121.164	121.294
C8–N1–C9	111.948	110.761	126.219	126.219
N–C9–N2–C10	134.433	133.305	–	–
S–C9–N2	–	–	121.120	120.866
C11–C12–O	119.149	119.773	118.774	118.729
N2–C10–C11	116.497	117.226	119.632	119.416
C11–C12–C13	119.551	119.708	121.348	121.434
C13–C14–C15	120.353	120.435	120.359	120.372
C15–C16–C17	120.031	120.004	119.965	119.986
C13–C18–C17	120.301	120.315	120.271	120.249
C19–C20–C21	120.959	120.826	120.368	120.257
C22–C23–C24	120.345	120.342	120.130	120.157
C8–C11–C12–O	60.341	49.667	39.617	39.617
C1–C2–C3–C4	−179.952	−179.875	−178.524	−178.898
C7–C6–C5–C8	179.475	−179.644	178.384	179.853
C5–C8–N1–C9	133.249	125.255	101.833	103.701
N–C9–N2–C10	169.358	166.365	–	–
S–C9–N2–C10	–	–	−171.249	−170.308
C10–C19–C20–C21	−179.575	−179.987	177.907	177.973
N2–C10–C19–C24	39.085	44.561	52.437	54.477
C12–C13–C14–C15	−178.151	−177.517	−176.595	−176.379
C12–C13–C18–C17	177.624	176.693	175.380	175.127

the geometry. The changes in the bond lengths are less than 0.014 and 0.02 Å for BCPTI and BTPTT, respectively. This suggests that protonation has minimal influence on the bond lengths of the inhibitors. The bond angles vary (in both directions) by <3° in both structures with the exception of the C8–C11–C12–O, C5–C8–N1–C9 and N2–C10–C19–C24 in BCPTI structure. The lengthening of C1=O1 (1.225 Å) and C9–S (1.695 Å) bond distances in their

Table 2 The quantum chemical descriptors of the BCPTI and BTPTT

Molecular descriptors	Parameter	BCPTI=BC		BTPTT=BT		Comments	
		Gas	Liquid	Gas	Liquid	Gas	Liquid
HOMO(eV)	-	−4.631	−6.683	−5.979	−6.384	BC>BT	BT>BC
LUMO(eV)	-	−2.192	−2.332	−2.283	−2.415	BC>BT	BC>BT
ΔE(eV)	-	2.439	4.351	3.696	3.969	BT>BC	BC>BT
Ionization Potential(IP)							
IP=[E(+1)-E(0)][a]	Energetic	5.865	6.772	7.533	5.615	BT>BC	BC>BT
IP=-E_{HOMO}[b]	Orbital	4.631	6.683	5.979	6.384	BT>BC	BC>BT
Electron Affinity(EA)(eV)							
EA=[E(0)-E(-1)][c]	Energetic	0.909	2.489	0.972	0.453	BT>BC	BT>BC BT>BC
EA=-E_{LUMO}[a]	Orbital	2.192	2.332	2.283	2.415	BT>BC	
Global hardness(η)(eV)	Energetic	2.479	2.141	3.28	2.581	BT>BC	BT>BC BC>BT
η=(I-A)/2[d]	Orbital	1.219	2.175	1.848	1.984	BT>BC	
Chemical potential(χ)(eV)	Energetic	3.386	4.63	4.252	3.034	BT>BC	BC>BT BC>BT
χ (I+A)/2[d]	Orbital	3.411	4.507	4.131	4.399	BT>BC	
Global softness(σ)(eV)	Energetic	0.403	0.467	0.305	0.387	BC>BT	BC>BT BT>BC
σ=1/η[e]	Orbital	0.82	0.459	0.541	0.504	BC>BT	
Electrophilicity(ω)(eV)	Energetic	2.312	5.006	2.756	1.783	BT>BC	BC>BT BT>BC
ω=χ^2/2η[f]	Orbital	4.772	4.669	4.617	4.877	BC>BT	
Electrodonating(ω^-)(eV)	Energetic	4.315	7.589	5.292	3.623	BT>BC	BC>BT
ω^-=(3I+A)^2/16(I-A)[g]	Orbital	6.629	7.195	6.914	7.324	BT>BC	BT>BC
Electroaccepting(ω^+)(eV)	Energetic	0.929	2.958	1.04	0.589	BT>BC	BC>BT
ω^+=(I+3A)^2/16(I-A)[g]	Orbital	3.218	2.688	2.783	2.925	BC>BT	BT>BC
net electrophilicity($\Delta\omega^\pm$)(eV)	Energetic	5.244	10.547	6.333	4.212	BT>BC	BC>BT
$\Delta\omega^\pm$=(ω^++ ω^-)[h]	Orbital	9.847	9.883	9.697	10.249	BC>BT	BT>BC
back-donation(ΔE_T)(eV)	Energetic	−0.619	−0.535	−0.82	−0.645	BC>BT	BC>BT
ΔE_T= -η/4[i]	Orbital	−0.305	−0.544	−0.462	−0.496	BC>BT	BT>BC
Transferred electrons(ΔN)	Energetic	0.729	0.553	0.419	0.768	BC>BT	BT>BC
ΔN=(χ_{Fe}- χ_{inh})/2(η_{Fe}+η_{inh})[m]	Orbital	1.471	0.573	0.776	0.655	BC>BT	BT>BC
Total Negative Charge(TNC)	-	7.658	8.139	8.344	8.077	BT>BC	BC>BT
Dipole moment(μ)(D)	-	7.827	14.565	5.807	7.954	BC>BT	BC>BT
ET (a.u)	-	−1316.222	−1316.265	−1509.846	−1509.865	BC>BT	BC>BT

[a] Ref. [48], [b] Ref. [49], [c] Ref. [50], [d] Ref. [51], [e] Ref. [52], [f] Ref. [53], [g] Ref. [40], [h] Ref. [41], [i] Ref. [42], [m] Ref. [27]

respective structures was noted in liquid phase which is probably the result of the high polarity of these bonds.

The quantum chemical descriptors are listed in Table 2 for the BCPTI and BTPTT molecules in gas and liquid phases. Table 2 descriptors were calculated by both energetic parameter and orbital parameter methods. The quantum chemical descriptors of the BCPTI and BTPTT molecules are not similar in gas and liquid phases in particular the dipole moment of BCPTI compound.

The binding ability of the BCPTI and BTPTT inhibitors to a metal surface increases with increasing HOMO and decreasing LUMO energies. The higher the value of E_{HOMO} becomes, the lower will be the capability of an inhibitor to accept electrons because the E_{HOMO} describes the electron-donating ability of the inhibitor. The energy of the LUMO indicates the ability of a molecule to accept electrons and thus the lower the value of E_{LUMO} becomes, the more probable that the molecule would accept electrons. Table 2 shows BCPTI and BTPTT have similar E_{HOMO} in gas and liquid phases but the E_{LUMO} of BTPTT is lower than the E_{LUMO} of BCPTI in both phases.

The gap between the HOMO and LUMO energy levels of the BCPTI and BTPTT molecules is a function of reactivity of the inhibitors with a metallic surface. The BCPTI and BTPTT have similar energy gaps in gas phase but BTPTT has a lower energy gap in liquid phase. The

Table 3 A pair of quantum chemical parameters utilized to derive the multiple regression Eq. (1) that correlates the theoretically estimated and the experimentally determined inhibition efficiencies, for BCPTI

Equation	Multiple regression equations
$Ie_{cal}\% = A + \frac{B_1 X_1}{C_1}$	**Gas**
	$8.509 \times 10^1 - 5.695 \times 10^{-4}\chi/C_1$
	$8.509 \times 10^1 + 4.164 \times 10^{-4}\text{HOMO}/C_1$
	$8.509 \times 10^1 + 8.797 \times 10^{-4}\text{LUMO}/C_1$
	$8.509 \times 10^1 - 7.906 \times 10^{-4}\Delta E/C_1$
	Liquid
	$8.509 \times 10^1 - 4.165 \times 10^{-4}\chi/C_1$
	$8.509 \times 10^1 + 2.885 \times 10^{-4}\text{HOMO}/C_1$
	$8.509 \times 10^1 + 8.269 \times 10^{-4}\text{LUMO}/C_1$
	$8.509 \times 10^1 - 4.431 \times 10^{-4}\Delta E/C_1$
$Ie_{cal}\% = A + \frac{B_1 X_1}{C_1} + \frac{B_2 X_2}{C_2^2}$	**Gas**
	$8.865 \times 10^1 - 1.584 \times 10^{-3}\chi/C_1 + 4.567 \times 10^{-8}\mu/C_2^2$
	$8.865 \times 10^1 - 2.199 \times 10^{-3}\Delta E/C_1 + 1.048 \times 10^{-7}\chi/C_2^2$
	$8.865 \times 10^1 + 1.158 \times 10^{-3}\text{HOMO}/C_1 - 1.620 \times 10^{-7}\text{LUMO}/C_2^2$
	$8.865 \times 10^1 - 1.584 \times 10^{-3}\chi/C_1 + 1.049 \times 10^{-7}\chi/C_2^2$
	Liquid
	$8.865 \times 10^1 - 1.158 \times 10^{-3}\chi/C_1 + 2.438 \times 10^{-8}\mu/C_2^2$
	$8.865 \times 10^1 - 1.233 \times 10^{-3}\Delta E/C_1 + 7.669 \times 10^{-8}\chi/C_2^2$
	$8.865 \times 10^1 + 8.028 \times 10^{-4}\text{HOMO}/C_1 - 1.523 \times 10^{-7}\text{LUMO}/C_2^2$
	$8.865 \times 10^1 - 1.158 \times 10^{-3}\chi/C_1 + 7.669 \times 10^{-8}\chi/C_2^2$
$Ie_{cal}\% = A + \frac{B_1 X_1}{C_1} + \frac{B_2 X_2}{C_2^2} + \frac{B_3 X_3}{C_3^3}$	**Gas**
	$9.108 \times 10^1 - 2.889 \times 10^{-3}\chi/C_1 + 2.309 \times 10^{-7}\mu/C_2^2 - 4.273 \times 10^{-11}\Delta E/C_3^3$
	$9.108 \times 10^1 - 2.889 \times 10^{-3}\chi/C_1 - 8.247 \times 10^{-7}\text{LUMO}/C_2^2 + 2.250 \times 10^{-11}\text{HOMO}/C_3^3$
	$9.108 \times 10^1 + 4.463 \times 10^{-3}\text{LUMO}/C_1 - 3.904 \times 10^{-7}\text{HOMO}/C_2^2 - 4.273 \times 10^{-11}\Delta E/C_3^3$
	Liquid
	$3.486 \times 10^{-10}\Delta E$
	$9.108 \times 10^1 - 2.170 \times 10^{-3}\chi/C_1 + 1.241 \times 10^{-7}\mu/C_2^2 - 2.395 \times 10^{-11}\Delta E/C_3^3$
	$9.108 \times 10^1 - 2.170 \times 10^{-3}\chi/C_1 - 7.752 \times 10^{-7}\text{LUMO}/C_2^2 + 1.559 \times 10^{-11}\text{HOMO}/C_3^3$
	$9.108 \times 10^1 + 4.195 \times 10^{-3}\text{LUMO}/C_1 - 2.705 \times 10^{-7}\text{HOMO}/C_2^2 - 2.395 \times 10^{-11}\Delta E/C_3^3$
$Ie_{cal}\% = A + \frac{B_1 X_1}{C_1} + \frac{B_2 X_2}{C_2^2} + \frac{B_3 X_3}{C_3^3} + \frac{B_4 X_4}{C_4^4}$	**Gas**
	$9.255 \times 10^1 - 4.276 \times 10^{-3}\chi/C_1 + 6.387 \times 10^{-7}\mu/C_2^2 - 3.154 \times 10^{-10}\Delta E/C_3^3 - 8.456 \times 10^{-15}\text{HOMO}$
	$9.255 \times 10^1 - 4.276 \times 10^{-3}\chi/C_1 - 2.280 \times 10^{-6}\text{LUMO}/C_2^2 - 3.154 \times 10^{-10}\Delta E/C_3^3 - 8.455 \times 10^{-15}\text{HOMO}/C_4^4$
	Liquid
	$9.255 \times 10^1 - 3.213 \times 10^{-3}\chi/C_1 + 3.432 \times 10^{-7}\mu/C_2^2 - 1.768 \times 10^{-10}DeltaE/C_3^3 - 5.859 \times 10^{-15}\text{HOMO}/C_4^4$
	$9.255 \times 10^1 - 3.213 \times 10^{-3}\chi/C_1 - 2.144 \times 10^{-6}\text{LUMO}/C_2^2 - 1.768 \times 10^{-10}\Delta E/C_3^3 - 5.859 \times 10^{-15}\text{HOMO}/C_4^4$

Table 4 A pair of quantum chemical parameters utilized to derive the multiple regression Eq. (1) that correlates the theoretically estimated and the experimentally determined inhibition efficiencies, for BTPTT

Equation	Multiple regression equations
$\mathrm{Ie_{cal}}\% = A + \frac{B_1 X_1}{C_1}$	**Gas**
	$9.061 \times 10^1 - 3.388 \times 10^{-4}\chi/C_1$
	$9.061 \times 10^1 + 2.398 \times 10^{-4}\mathrm{HOMO}\ /C_1$
	$9.061 \times 10^1 + 6.281 \times 10^{-4}\mathrm{LUMO}/C_1$
	$9.061 \times 10^1 - 3.879 \times 10^{-4}\Delta E/C_1$
	Liquid
	$9.061 \times 10^1 - 4.726 \times 10^{-4}\chi/C_1$
	$9.061 \times 10^1 + 2.246 \times 10^{-4}\mathrm{HOMO}/C_1$
	$9.061 \times 10^1 + 5.937 \times 10^{-4}\mathrm{LUMO}/C_1$
	$9.061 \times 10^1 - 3.613 \times 10^{-4}\Delta E/C_1$
$\mathrm{Ie_{cal}}\% = A + \frac{B_1 X_1}{C_1} + \frac{B_2 X_2}{C_2^2}$	**Gas**
	$9.326 \times 10^1 - 9.383 \times 10^{-4}\chi/C_1 + 4.547 \times 10^{-8}\mu/C_2^2$
	$9.326 \times 10^1 - 1.079 \times 10^{-3}\Delta E/C_1 + 6.209 \times 10^{-8}\chi/C_2^2$
	$9.326 \times 10^1 + 6.672 \times 10^{-4}\mathrm{HOMO}/C_1 - 1.156 \times 10^{-7}\mathrm{LUMO}/C_2^2$
	$9.326 \times 10^1 - 9.383 \times 10^{-4}\chi/C_1 + 6.209 \times 10^{-8}\chi/C_2^2$
	Liquid
	$9.326 \times 10^1 - 1.315 \times 10^{-3}\chi/C_1 + 3.319 \times 10^{-8}\mu/C_2^2$
	$9.326 \times 10^1 - 1.005 \times 10^{-3}\Delta E/C_1 + 8.730 \times 10^{-8}\chi/C_2^2$
	$9.326 \times 10^1 + 6.249 \times 10^{-4}\mathrm{HOMO}/C_1 - 1.093 \times 10^{-7}\mathrm{LUMO}/C_2^2$
	$9.326 \times 10^1 - 1.315 \times 10^{-3}\chi/C_1 + 8.703 \times 10^{-8}\chi/C_2^2$
$\mathrm{Ie_{cal}}\% = A + \frac{B_1 X_1}{C_1} + \frac{B_2 X_2}{C_2^2} + \frac{B_3 X_3}{C_3^3}$	**Gas**
	$9.507 \times 10^1 - 1.711 \times 10^{-3}\chi/C_1 + 2.315 \times 10^{-7}\mu/C_2^2 - 2.096 \times 10^{-11}\Delta E/C_3^3$
	$9.507 \times 10^1 - 1.711 \times 10^{-3}\chi/C_1 - 5.888 \times 10^{-7}\mathrm{LUMO}/C_2^2 + 1.296 \times 10^{-11}\mathrm{HOMO}/C_3^3$
	$9.507 \times 10^1 + 3.186 \times 10^{-3}\mathrm{LUMO}C_i - 2.248 \times 10^{-7}\mathrm{HOMO}/C_2^2 - 2.096 \times 10^{-11}\Delta E/C_3^3$
	Liquid
	$9.507 \times 10^1 - 2.398 \times 10^{-3}\chi/C_1 + 1.690 \times 10^{-7}\mu/C_2^2 - 1.952 \times 10^{-11}\Delta E/C_3^3$
	$9.507 \times 10^1 - 2.398 \times 10^{-3}\chi/C_1 - 5.566 \times 10^{-7}\mathrm{LUMO}/C_2^2 + 1.214 \times 10^{-11}\mathrm{HOMO}/C_3^3$
	$9.507 \times 10^1 + 3.012 \times 10^{-3}\mathrm{LUMO}\ C_i - 2.105 \times 10^{-7}\mathrm{HOMO}/C_2^2 - 1.952 \times 10^{-11}\Delta E/C_3^3$

binding ability of the inhibitors to a metal surface increases with decreasing energy gap. This means that the BTPTT molecule could perform better as a corrosion inhibitor in liquid phase.

Ionization potential (IP) is a basic descriptor of the chemical reactivity of atoms and molecules. IP is the minimum energy required to remove an electron from an atom. Chemical potential indicates the molecular capability of accepting electrons. A low IP indicates less energy needed to remove electrons from a system and also low stability. Similarly, a low chemical potential indicates low stability. Table 2 shows BCPTI and BTPTT have low ionization energies in gas and liquid phases.

The absolute hardness and softness are important properties for measuring a molecular stability and reactivity. Table 2 shows that BCPTI has a lower hardness and a higher softness in gas and liquid phases (except for values obtained by orbital parameter method) which reflect the high reactivity of BCPTI as compared with BTPTT.

A hard molecule has a large energy gap and a soft molecule has a small energy gap. Soft molecules are more reactive than hard ones because they could easily offer electrons to an electron acceptor. BCPTI is a soft molecule in both gas and liquid phases. It has a small energy gap in gas phase but a large energy gap in liquid phase. BCPTI molecule is more reactive than BTPTT in gas phase but is less reactive than BTPTT in liquid phase as indicated by calculations based on orbital parameter. The ability of an inhibitor molecule to accept electrons is described by its electrophilicity index. Electrophilicity is a measure of the energy stabilization after a system accepts additional amount of electron charge from its environment.

Based on energetic parameter calculations, BCPTI has a lower value of electrophilicity in gas phase and therefore

Table 5 Experimental inhibition efficiencies of BCPTI and BTPTT and computational inhibition efficiencies at different concentrations using Eqs. (2–5)

Inhibitor	Concentration (mol/dm³)	Inhibition efficiency (Ie_exp %)[a]	Inhibition efficiency (Ie_cal %)							
			$A + \frac{B_1X_1}{C_1}$		$A + \frac{B_1X_1}{C_1} + \frac{B_2X_2}{C_2}$		$A + \frac{B_1X_1}{C_1} + \frac{B_2X_2}{C_2} + \frac{B_3X_3}{C_3}$		$A + \frac{B_1X_1}{C_1} + \frac{B_2X_2}{C_2} + \frac{B_3X_3}{C_3} + \frac{B_4X_4}{C_4}$	
			Gas	Liquid	Gas	Liquid	Gas	Liquid	Gas	Liquid
BCPTI	0.0001	69	65.80	65.80	70.50	70.50	69.822	69.822	69.874	69.874
	0.0005	80	5	5	9	9	77.917	77.917	78.058	78.058
	0.001	82	81.23	81.23	79.34	79.34	83.007	83.007	82.340	82.340
	0.005	90	84.704	84.704	87.593	87.593	89.201	89.201	89.850	89.850
			$R^2 = 0.864$	$R^2 = 0.864$	$R^2 = 0.969$	$R^2 = 0.969$	$R^2 = 0.973$	$R^2 = 0.973$	$R^2 = 0.980$	$R^2 = 0.980$
BTPTT	0.0001	78	76.27	76.27	79.77	79.77	79.261	79.261	–	–
	0.0005	86	4	4	1	1	85.280	85.280		
	0.001	91	87.74	87.74	86.33	86.33	89.064	89.064		
	0.005	93	90.326	90.326	92.475	92.475	93.670	93.670		
			$R^2 = 0.914$	$R^2 = 0.702$	$R^2 = 0.990$	$R^2 = 0.990$	$R^2 = 0.958$	$R^2 = 0.958$		

The R^2 values are also reported

[a] Inhibiting efficiency determined as reported in [29]

this molecule is a stronger nucleophile than BTPTT but based on orbital parameter calculations, the BCPTI is a weaker nucleophile than BTPTT in liquid phase. A larger electroaccepting value corresponds to a better capability of accepting charge, whereas a smaller value of electrodonating value of a system makes it a better electron donor [47].

The calculated electrodonating, electroaccepting and net electrophilicity values of the BCPTI and BTPTT inhibitors are listed in Table 2. The energy parameter indicates BCPTI is a better electron donor than BTPTT in gas phase and the orbital parameter indicates BCPTI is also a better electron donor than BTPTT in liquid phase. In contrast to this, the energy parameter indicates BTPTT molecule has a better capability of accepting charge in gas phase and the orbital parameter indicates BTPTT molecule has also a better capability of accepting charge in liquid phase. The total electrophilicity indicates BCPTI is the strongest nucleophile in gas phase if energy parameter is applied and also is the strongest nucleophile in liquid phase if orbital parameter is applied. In contrast to this, BTPTT molecule is the strongest nucleophile in gas phase if orbital parameter is applied and also is the strongest nucleophile in liquid phase if energy parameter is applied. These are similar to the results obtained by the electrophilicity index. The calculated back-donation (ΔE_T) values of the inhibitors are listed in Table 2. This Table shows the back-donation (ΔE_T) values are similar to global softness values (σ).

The trend of electrons' donation within a set of inhibitors is described by the fraction of electrons transferred (ΔN). If ΔN is below 3.6 eV, then the inhibition efficiency increases with increasing ω^- ability at the mild steel interface [48]. Table 2 shows that all values of the ΔN are below 3.6 eV and the BCPTI and BTPTT have the highest values of ΔN in gas and liquid phases. Because iron is the major constituent of austenitic stainless steel, the theoretical values of the iron electronegativity ($\chi_{Fe} = 7$ eV) and the iron global hardness ($\eta_{Fe} = 0$) were used to compute ΔN for the various Hamiltonians [49].

The calculations show that BTPTT and BCPTI have the highest TNC values in gas and liquid phases. The adsorption of the inhibitor onto the mild steel surface is enhanced at higher TNC values. The TNC values of the BTPTT and BCPTI molecules are higher in liquid phase than in gas phase.

Information about the polarity of a molecule describes its μ. In general, there is no significant relationship between the μ values and inhibition efficiencies. In some systems, the μ appears to increase with increasing inhibition efficiencies [50] while in some other systems the μ appears to decrease as the inhibition efficiency increases [51]. Table 2 shows that BCPTI has the highest μ value in gas and liquid phases and the highest molecular mass. There is a

Fig. 3 The plots of experimental inhibition efficiencies of BCPTI and computational inhibition efficiencies at different concentrations using Eqs. (2–5). The R2 values are also reported
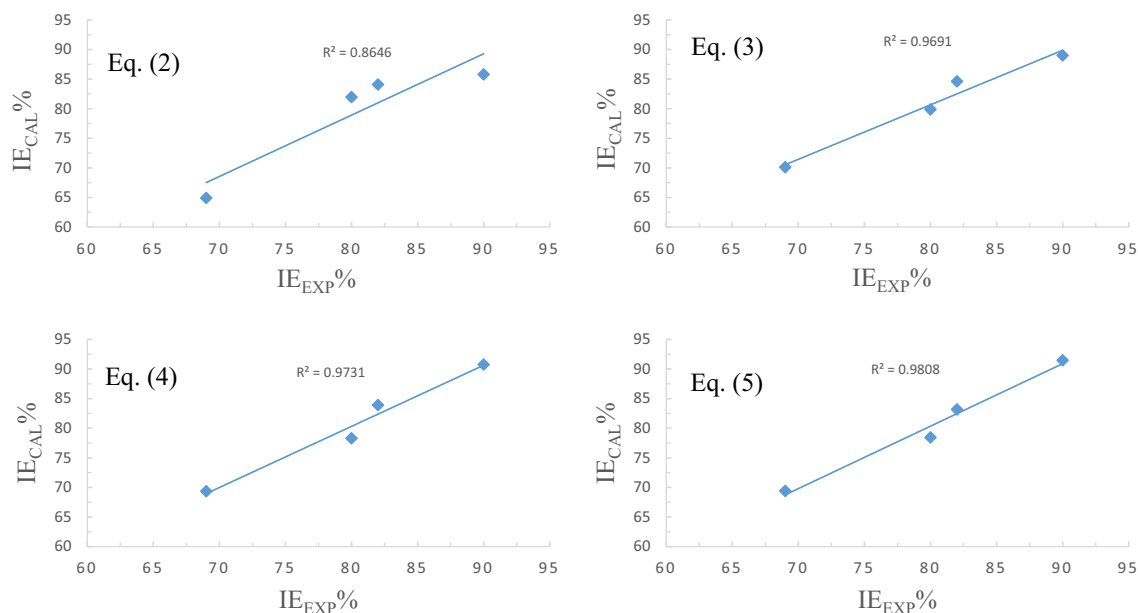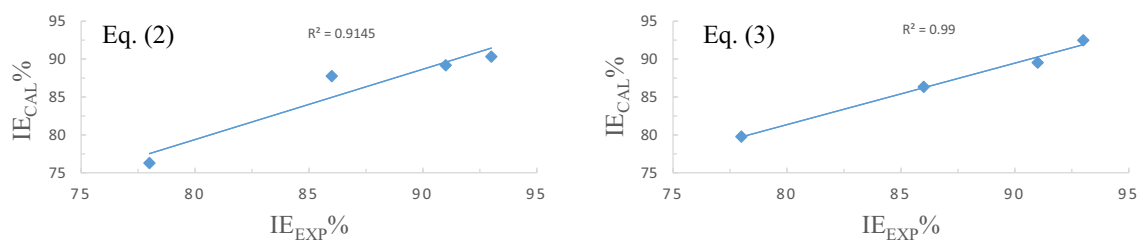

Fig. 4 The plots of experimental inhibition efficiencies of BTPTT and computational inhibition efficiencies at different concentrations using Eqs. (2, 3). The R2 values are also reported

correlation between the molecular mass and the inhibition efficiency. As a molecular mass increases, its adsorption on a metal surface will increase. Inhibition efficiency increases as adsorption increases. It is clear from Table 2 that μ is higher in water than in gas and this is an indication of the polarization effect of the solvent on the inhibitor molecules. The difference between the μ values of BTPTT in gas and water is 2.02 but for BCPTI this difference is 6.61. This demonstrates that the polarization effect of the solvent on BCPTI molecule is more than its effect on the BTPTT molecule. This is because BCPTI has two oxygen atoms and a nitrogen atom but BTPTT has a sulfur atom.

From the computed results obtained for gas and liquid phases (Table 2), we can easily notice the stabilization effect of the solvent on the significant decrease of the E_T values of the two inhibitors. The E_T values show that BCPTI is more stable than BTPTT.

QSAR consideration

The QSAR method was used to correlate the inhibition efficiencies of the BCPTI and BTPTT with their molecular structures in gas and liquid phases. Attempts were made to establish a relationship between the experimental corrosion inhibition efficiencies and the calculated quantum chemical parameters. To obtain equations that are useful in predicting inhibition efficiency (Ie_{cal}) from the concentrations of the inhibitors and their quantum chemical parameters, Eq. (1) has been proposed to calculate the Ie_{cal}.

$$Ie_{calc}\% = A + \frac{B_1 X_1}{C_1} + \frac{B_2 X_2}{C_2^2} + \frac{B_3 X_3}{C_3^3} + \cdots \in + \frac{B_n X_n}{C_n^n}, \quad (1)$$

where A and B_n are constants obtained by regression analysis, X_n parameters are the independent variables consisting of quantum chemical values and C_n parameters are the

Table 6 Calculated Mulliken atomic charges for BCPTI using DFT at the B3LYP/++6-31G (d, p) basis set

Atom	QN		QN + 1		QN − 1	
	Gas	Liquid	Gas	Liquid	Gas	Liquid
C1	0.294	0.305	0.304	0.301	0.286	0.309
C2	0.701	0.673	0.666	0.635	0.795	0.799
C3	−0.692	−0.649	−0.722	−0.656	−0.716	−0.676
C4	−0.163	−0.224	−0.224	−0.266	−0.139	−0.159
C5	0.996	0.927	1.004	0.949	0.952	0.954
C6	−0.998	−1.081	−0.991	−1.076	−0.939	−1.052
C7	−0.548	−0.596	−0.554	−0.640	−0.510	−0.568
C8	−0.293	−0.466	−0.258	−0.428	−0.240	−0.367
C9	−0.050	0.005	−0.036	0.017	−0.112	−0.064
C10	−0.983	−0.217	−1.040	−0.253	−0.844	−0.223
C11	0.741	0.205	0.777	0.242	0.629	0.237
C12	−0.897	−0.672	−0.953	−0.676	−0.816	−0.693
C13	0.630	0.497	0.752	0.532	0.588	0.482
C14	0.428	0.220	0.332	0.133	0.382	0.208
C15	−0.425	−0.507	−0.425	−0.508	−0.423	−0.503
C16	−0.387	−0.386	−0.420	−0.435	−0.384	−0.379
C17	−0.099	−0.088	−0.133	−0.147	−0.077	−0.063
C18	−0.504	−0.298	−0.534	−0.378	−0.492	−0.308
C19	0.959	0.657	0.947	0.648	0.938	0.719
C20	−0.770	−0.529	−0.701	−0.471	−0.744	−0.567
C21	−0.361	−0.410	−0.374	−0.426	−0.334	−0.391
C22	−0.324	−0.357	−0.341	−0.376	−0.294	−0.335
C23	−0.267	−0.285	−0.276	−0.299	−0.253	−0.273
C24	−0.065	−0.088	−0.137	−0.163	−0.024	−0.056
N1	0.205	0.221	0.202	0.205	0.198	0.258
N	−0.291	−0.373	−0.351	−0.420	−0.196	−0.274
N2	−0.063	−0.061	−0.066	−0.081	−0.045	−0.021
O1	−0.314	−0.410	−0.359	−0.433	−0.255	−0.350
O2	−0.200	−0.232	−0.215	−0.242	−0.183	−0.208
O	−0.119	−0.210	−0.235	−0.398	−0.104	−0.181

Table 7 Calculated Mulliken atomic charges for BTPTT using DFT at the B3LYP/++6-31G (d, p) basis set

Atom	Q_N		QN + 1		QN − 1	
	Gas	Liquid	Gas	Liquid	Gas	Liquid
C1	−0.514	−0.538	−0.547	−0.541	−0.479	−0.542
C2	0.422	0.349	0.467	0.323	0.385	0.336
C3	−0.475	−0.502	−0.494	−0.555	−0.446	−0.509
C4	−0.418	−0.221	−0.384	−0.263	−0.384	−0.207
C5	1.164	1.182	1.201	1.217	1.166	1.259
C6	−0.376	−0.363	−0.391	−0.407	−0.357	−0.399
C7	−0.692	−0.703	−0.726	−0.703	−0.671	−0.696
C8	0.140	0.160	0.161	0.264	0.116	−0.001
C9	0.278	0.232	0.322	0.235	0.248	0.296
C10	−0.286	−0.318	−0.321	−0.336	−0.280	−0.334
C11	−0.288	0.154	−0.217	0.103	−0.325	0.088
C12	−1.003	−1.201	−1.092	−1.120	−0.970	−1.135
C13	0.875	0.696	0.985	0.624	0.894	0.720
C14	−0.984	−0.517	−0.994	−0.552	−1.019	−0.545
C15	−0.271	−0.188	−0.317	−0.224	−0.252	−0.196
C16	−0.247	−0.301	−0.289	−0.366	−0.236	−0.314
C17	−0.388	−0.469	−0.387	−0.478	−0.386	−0.490
C18	1.038	0.619	0.927	0.481	1.047	0.588
C19	0.790	0.767	0.828	0.744	0.808	0.831
C20	−0.570	−0.575	−0.504	−0.608	−0.567	−0.659
C21	−0.430	−0.414	−0.464	−0.449	−0.412	−0.425
C22	−0.240	−0.333	−0.265	−0.366	−0.225	−0.341
C23	−0.376	−0.410	−0.383	−0.436	−0.372	−0.408
C24	0.050	−0.043	−0.054	−0.095	0.077	−0.069
N1	−0.187	−0.217	−0.214	−0.309	−0.164	−0.200
N2	0.030	0.037	0.025	−0.039	0.085	0.083
O	−0.151	−0.230	−0.278	−0.457	−0.103	−0.211
S	−0.835	−1.002	−1.026	−1.135	−0.530	−0.657

inhibitor concentrations. The Eq. (1) shows that inhibition efficiency strongly depends on density parameter. To simplify the Eq. (1), only the first four terms were used.

$$Ie_{calc}\% = A + \frac{B_1 X_1}{C_1} \tag{2}$$

$$Ie_{calc}\% = A + \frac{B_1 X_1}{C_1} + \frac{B_2 X_2}{C_2^2} \tag{3}$$

$$Ie_{calc}\% = A + \frac{B_1 X_1}{C_1} + \frac{B_2 X_2}{C_2^2} + \frac{B_3 X_3}{C_3^3} \tag{4}$$

$$Ie_{calc}\% = A + \frac{B_1 X_1}{C_1} + \frac{B_2 X_2}{C_2^2} + \frac{B_3 X_3}{C_3^3} + \frac{B_4 X_4}{C_4^4}. \tag{5}$$

Equations (2–5) were utilized to correlate the composite index of the quantum chemical parameters with the experimental inhibition efficiency (I_{exp} %) of the studied inhibitors. Tables 3 and 4 show the fitted equations obtained using multiple regression analyses. Table 5; Figs. 3 and 4 show that the Ie$_{cal}$ % values of BCPTI and BTPTT, calculated by using Eqs. (5) and (3), agree well with the experimental results.

Local molecular reactivity

Selectivity parameters indicate the regions of a molecule that are likely to interact with a metal surface. These parameters include the Mulliken atomic charges, distribution of frontier molecular orbital and the Fukui functions [52]. An atom with the highest negative partial atomic charge interacts most strongly with a metal surface through a donor–acceptor type of interaction because it represents the site with the highest electron density. Tables 6 and 7

Table 8 Calculated Fukui functions for BCPTI using DFT at the B3LYP/++6-31G (d, p) basis set

Atom	$|f^+|$		$|f^-|$		$|\Delta f|$	
	Gas	Liquid	Gas	Liquid	Gas	Liquid
C1	0.010	0.004	0.008	0.004	0.003	0.000
C2	0.035	0.038	0.094	0.126	0.059	0.088
C3	0.030	0.007	0.024	0.026	0.054	0.033
C4	0.060	0.042	0.024	0.065	0.036	0.023
C5	0.008	0.022	0.044	0.026	0.036	0.048
C6	0.007	0.005	0.059	0.029	0.066	0.033
C7	0.006	0.043	0.039	0.029	0.033	0.015
C8	0.036	0.038	0.054	0.099	0.089	0.137
C9	0.015	0.012	0.061	0.069	0.047	0.056
C10	0.056	0.036	0.140	0.006	0.083	0.042
C11	0.036	0.037	0.112	0.032	0.076	0.069
C12	0.056	0.005	0.081	0.022	0.024	0.026
C13	0.122	0.035	0.042	0.015	0.080	0.020
C14	0.095	0.087	0.045	0.011	0.141	0.098
C15	0.001	0.001	0.002	0.004	0.003	0.004
C16	0.033	0.049	0.003	0.007	0.030	0.042
C17	0.034	0.059	0.021	0.025	0.012	0.034
C18	0.030	0.080	0.012	0.010	0.018	0.089
C19	0.011	0.010	0.020	0.062	0.032	0.052
C20	0.069	0.058	0.026	0.038	0.095	0.020
C21	0.013	0.015	0.027	0.020	0.014	0.004
C22	0.016	0.019	0.030	0.022	0.014	0.003
C23	0.009	0.014	0.015	0.012	0.006	0.002
C24	0.072	0.075	0.041	0.032	0.031	0.043
N1	0.003	0.016	0.007	0.037	0.010	0.021
N	0.060	0.047	0.095	0.098	0.036	0.051
N2	0.003	0.020	0.018	0.039	0.015	0.019
O1	0.045	0.023	0.059	0.059	0.014	0.036
O2	0.015	0.010	0.017	0.024	0.002	0.014
O	0.117	0.188	0.015	0.029	0.102	0.159

Table 9 Calculated Fukui functions for BTPTT using DFT at the B3LYP/++6-31G (d, p) basis set

Atom	$|f^+|$		$|f^-|$		$|\Delta f|$	
	Gas	Liquid	Gas	Liquid	Gas	Liquid
C1	0.034	0.003	0.035	0.003	0.001	0.006
C2	0.045	0.026	0.037	0.012	0.009	0.038
C3	0.019	0.053	0.029	0.007	0.010	0.060
C4	0.034	0.042	0.034	0.014	0.068	0.028
C5	0.037	0.035	0.002	0.076	0.039	0.111
C6	0.015	0.045	0.018	0.036	0.003	0.081
C7	0.034	0.001	0.021	0.007	0.013	0.007
C8	0.020	0.105	0.024	0.161	0.003	0.056
C9	0.043	0.003	0.031	0.063	0.012	0.066
C10	0.035	0.018	0.006	0.016	0.029	0.034
C11	0.071	0.051	0.037	0.066	0.034	0.117
C12	0.089	0.081	0.033	0.066	0.056	0.147
C13	0.109	0.073	0.018	0.024	0.127	0.049
C14	0.010	0.035	0.035	0.028	0.045	0.062
C15	0.046	0.036	0.019	0.008	0.027	0.044
C16	0.042	0.066	0.011	0.013	0.031	0.079
C17	0.000	0.009	0.002	0.021	0.002	0.030
C18	0.111	0.138	0.009	0.031	0.102	0.169
C19	0.038	0.023	0.018	0.063	0.056	0.041
C20	0.066	0.033	0.002	0.084	0.068	0.117
C21	0.033	0.035	0.019	0.010	0.015	0.045
C22	0.026	0.034	0.015	0.009	0.011	0.043
C23	0.007	0.027	0.004	0.002	0.003	0.025
C24	0.104	0.052	0.027	0.025	0.078	0.077
N1	0.027	0.091	0.024	0.017	0.004	0.074
N2	0.006	0.075	0.055	0.047	0.049	0.029
O	0.126	0.227	0.049	0.019	0.077	0.208
S	0.191	0.133	0.305	0.346	0.114	0.213

report the Mulliken atomic charges of the atoms in the anionic (Q_{N+1}), neutral (Q_N) and cationic (Q_{N-1}) states of the studied compounds in both phases. Q_{N+1} is an anion with an electron added to the LUMO of its neutral molecule. Q_{N-1} is a cation with an electron removed from the HOMO of its neutral molecule.

The highest negative charges are on C6 and C10 atoms of the BCPTI in its gas phase and on C10 atom in its liquid phase. High negative charges exist on oxygen and nitrogen atoms of the BCPTI.

The highest negative charges are on C12 and the heteroatom S of the BTPTT in both phases. Because heteroatoms have lone pair of electrons, these lone pair of electrons could be donated to the vacant *s* or partially filled *d* orbital of a metal and thereby facilitate the adsorption of

the inhibitor on the metal surface. BCPTI has more heteroatoms than BTPTT. Therefore, BCPTI has a higher charge density and would interact with a metal surface at more sites than BTPTT. BTPTT has the highest sites for adsorption onto a metal surface because it has the highest number of heteroatoms.

The Fukui indices permit the distinction between the reactive regions of a molecule, the nucleophilic and electrophilic behaviors of a molecule and the chemical reactivity. These functions can be given by Eqs. (6) and (7) [53]:

$$f^+ = Q_{N+1} - Q_N \tag{6}$$

$$f^+ = Q_N - Q_{N-1}. \tag{7}$$

The calculated values of the Fukui functions for the non-hydrogen atoms are reported in Tables 8 and 9.

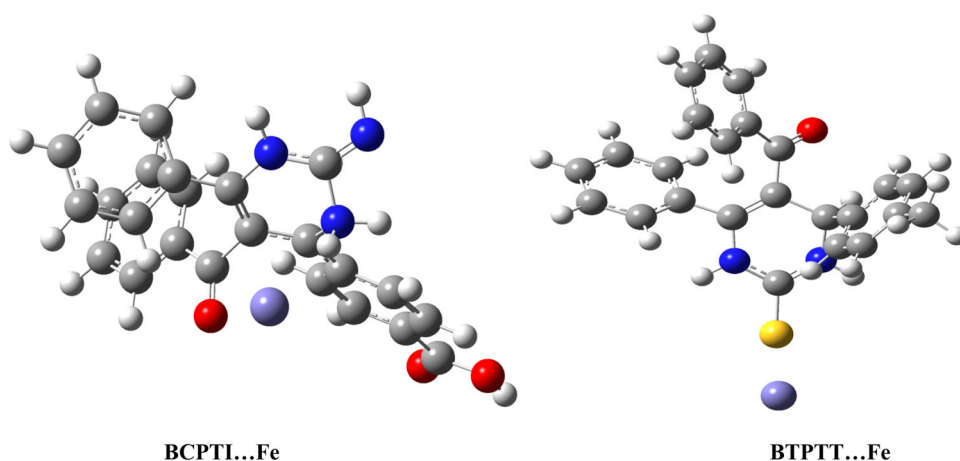**Fig. 5** The structures of Fe–inhibitor complexes (using DFT/B3LYP/6-311++G (d, p))

BCPTI…Fe   **BTPTT…Fe**

Table 10 The interaction energy and the energy binding between the metal and the inhibitor

Complex	Bond type	Inhibitor···Fe separation distance		$E_{\text{interaction}}$ (eV)		E_{binding} (eV)	
		Gas	Liquid	Gas	Liquid	Gas	Liquid
BCPTI···Fe	O···Fe	1.882	1.902	−3.319	−3.259	3.319	3.259
	C10···Fe	3.784	3.813				
	C8···Fe	1.987	1.941				
	C6···Fe	2.106	2.126				
BTPTT···Fe	S···Fe	1.548	1.694	1.074	1.198	−1.074	−1.198

The maximum of f$^+$ corresponds to reactivity with respect to nucleophilic attack and the maximum of f^- shows the preferred site for adsorption of electrophilic agents. For BCPTI, the highest f$^+$ is associated with C13 and O atoms in gas phase and O atom in liquid phase and the highest f^- occurs at C10 and C11 atoms in gas phase and at C2 and C8 atoms in liquid phase. The BTPTT sites for nucleophilic attack are the S atoms in gas phase and O atoms in liquid phases. However, the BTPTT sites for electrophilic attack are only the S atoms in both gas and liquid phases.

The adsorption of inhibitors on austenitic stainless steel

Iron is the major element of the austenitic stainless steel. Therefore, the iron interaction with the inhibitor molecules should be investigated [26–28]. The binding capability of a metal on the inhibitors depends strongly on the electronic charge of the active site. The Mulliken atomic charges, distribution of frontier molecular orbital and the Fukui functions show that iron atom is located among C6, C8, C10 and O atoms of BCPTI molecule whereas in BTPTT molecule, the iron atom Therefore, BCPTI and BTPTT were allowed to interact with the Fe metal at the C6, C8, C10 and the S atom. The interaction energy between the inhibitor and the metal was then estimated as the difference between the energy of the complex ($E_{\text{Fe}-X}$) and the sum of the energy of the isolated inhibitor and isolated Fe atom ($E_X + E_{\text{Fe}}$) resulting in the equation: $E_{\text{interaction}} = E_{\text{Fe}-X} - (E_X + E_{\text{Fe}})$. The binding energy of the inhibitor molecule is the negative value of interaction energy [54].

The optimized inhibitor···Fe complexes are shown in Fig. 5. The inhibitor···Fe separation distance, the calculated interaction and binding energy are reported in Table 10. The strong adsorption between the inhibitor molecules and the iron can be estimated as the larger negative values of interaction energy [55]. Table 10 shows that BCPTI has the highest interaction energy and therefore has the highest inhibition efficiency. From the theoretical point of view, the higher magnitude of BCPTI binding energy suggests a more stable adsorption and a higher inhibition efficiency system.

Conclusions

Quantum chemical calculations based on density functional theory method were performed on two pyrimidine derivatives which may be used as corrosion inhibitors for austenitic stainless steel. The quantum chemical properties of the two pyrimidine derivatives that are most relevant to

their potential action as corrosion inhibitors were calculated in gas and liquid phases for comparison purposes. Our results indicate computational data for liquid phase represent the experimental results better than the data for gas phase. The quantum chemical parameters of the inhibitors are different in gas and liquid phases and some of the same type parameters obtained by orbital method are different from those obtained by energy method. We have not been able to establish relationships between some of quantum chemical parameters, e.g., molecular softness and energy gap.

In this study, the corrosion inhibition capabilities of the BCPTI and BTPTT were investigated. We have made the following conclusions:

1. BTPTT has a smaller energy gap than BCPTI in liquid phase and therefore it is a better inhibitor.
2. Based on global softness, hardness and chemical potential obtained by energy method but excluding calculations obtained by orbital method, BCPTI is a better inhibitor than BTPTT in both gas and liquid phases.
3. Based on dipole moment and molecular mass, BCPTI is a better inhibitor than BTPTT in both gas and liquid phases.
4. An equation has been proposed to calculate the inhibition efficiency. The regression analyses fitted the Caliskan et al. experimental data well and the calculated inhibition efficiencies of the studied compounds were found to be close to their experimental corrosion inhibition efficiencies.
5. The adsorption of the studied compounds onto the steel surface shows that BCPTI inhibitor has a higher magnitude of binding energy than BTPTT.
6. Overall, BCPTI may be a better inhibitor than BTPTT.

References

1. Elayyachy M, Hammouti B, El Idrissi A (2005) New telechelic compounds as corrosion inhibitors for steel in 1 M HCl. Appl Surf Sci 249:176–182
2. Bouklah M, Hammouti B, Lagrenée M, Bentiss F (2006) Thermodynamic properties of 2,5-bis(4-methoxyphenyl)-1,3,4-oxadiazole as a corrosion inhibitor for mild steel in normal sulfuric acid medium. Corros Sci 48:2831–2842
3. Khatak HS, Baldev R (2002) Corrosion of austenitic stainless steels: mechanism, mitigation and monitoring, ASM International, Narosa Publishing House
4. Marshall P (1984) Austenitic stainless steels: microstructure and mechanical properties. Elsevier Applied Science Publishers Ltd, New York
5. Truman JE, Pirt KR (1997) A note on the corrosion produced under deposits of chlorides on austenitic stainless steel. Corros Sci 17:71–74
6. Craig DB (1995) Selection guidelines for corrosion resistant alloys in the oil and gas industry. NiDI Technical Series No. 10 073, Toronto, Ontario, Canada
7. Emregül KC, Atakol O (2003) Corrosion inhibition of mild steel with Schiff base compounds in 1 M HCl. Mater Chem Phys 82:188–193
8. Elayyachy M, El Idrissi A, Hammouti B (2006) New thio-compounds as corrosion inhibitor for steel in 1 M HCl. Corros Sci 48:2470–2479
9. Fouda AS, Ellithy AS (2009) Inhibition effect of 4-phenylthiazole derivatives on corrosion of 304L stainless steel in HCl solution. Corros Sci 51:868–875
10. Refaey SAM, Taha F, Abd El-Malak AM (2006) Corrosion and Inhibition of 316L stainless steel in neutral medium by 2-mercaptobenzimidazole. Int J Electrochem Sci 1:80–91
11. Selvakumar P, Balanaga Karthik B, Thangavelu C (2013) Corrosion inhibition study of stainless steel in acidic medium—an overview. Res J Chem Sci 3:87–95
12. Adnani ZE, Mcharfi M, Sfaira M, Benzakour M, Benjelloun AT, Touhami ME (2013) DFT theoretical study of 7-R-3methylquinoxalin-2(1H)-thiones (R = H; CH3; Cl) as corrosion inhibitors. Corros Sci 68:223–230
13. Kabanda MM, Murulana LC, Ozcan M, Karadag F, Dehri I, Obot IB, Ebenso EE (2010) Quantum chemical studies on the corrosion inhibition of mild steel by some triazoles and benzimidazole derivatives in acidic medium. Int J Electrochem Sci 7:5035–5056
14. Khaled KF (2008) Molecular simulation, quantum chemical calculations and electrochemical studies for inhibition of mild steel by triazoles. Electrochim Acta 53:3484–3492
15. Xia S, Qiu M, Yu L, Liu F, Zhao H (2008) Molecular dynamics and density functional theory study on relationship between structure of imidazoline derivatives and inhibition performance. Corros Sci 50:2021–2029
16. Elmsellem H, Aouniti A, Khoutoul M, Chetouani A, Hammouti B, Benchat N, Touzani R, Elazzouzi M (2014) Theoretical approach to the corrosion inhibition efficiency of some pyrimidine derivatives using DFT method of mild steel in HCl solution. J Chem Pharm Res 6(4):1216–1224
17. Udhayakala P, Rajendiran TV (2015) A theoretical evaluation on benzothiazole derivatives as corrosion inhibitors on mild steel. Der Pharma Chem 7(1):92–99
18. Ismaily AK, El Hajjaji F, Azaroual MA, Taleb M, Chetouani A, Hammouti B, Abrigach F, Khoutoul M, Abboud Y, Aouniti A, Touzani R (2014) Experimental and quantum chemical studies on corrosion inhibition performance of pyrazolic derivatives for mild steel in hydrochloric acid medium, correlation between electronic structure and inhibition efficiency. J Chem Pharm Res 6(7):63–81
19. Yadav M, Kumar S, Kumari N, Bahadur I, Ebenso EE (2015) Experimental and theoretical studies on corrosion inhibition effect of synthesized benzothiazole derivatives on mild steel in 15% HCl solution. Int J Electrochem Sci 10:602–624
20. Zarrouk A, Hammouti B, Lakhlifi T, Traisnel M, Vezin H, Bentiss F (2015) New 1H-pyrrole-2,5-dione derivatives as efficient organic inhibitors of carbon steel corrosion in hydrochloric acid medium: electrochemical, XPS and DFT studies. Corros Sci 90:572–584

21. Murulana LC, Kabandabc MM, Ebenso EE (2015) Experimental and theoretical studies on the corrosion inhibition of mild steel by some sulphonamides in aqueous HCl. RSC Adv 5:28743–28761

22. Saha SK, Dutta A, Ghosh P, Sukulc D, Banerjee P (2015) Adsorption and corrosion inhibition effect of Schiff base molecules on the mild steel surface in 1 M HCl medium: a combined experimental and theoretical approach. Phys Chem Chem Phys 17(8):5679–5690

23. Kayadibi F, Sagdinc SG, Kara YS (2015) Density functional theory studies on the corrosion inhibition of benzoin, benzil, benzoin-(4-phenylthiosemicarbazone) and benzil-(4-phenylthiosemicarbazone) of mild steel in hydrochloric acid. Prot Metals Phys Chem Surf 51(1):143–154

24. Odozi NW, Babalola JO, Ituen EB, Eseola AO (2015) Imidazole derivative as novel effective inhibitor of mild steel corrosion in aqueous sulphuric acid. Am J Phys Chem 4(1–1):1–9

25. Radillaa J, Negrón-Silvaa GE, Palomar-Pardavéb M, Romero-Romob M, Galvánc M (2013) DFT study of the adsorption of the corrosion inhibitor 2-mercaptoimidazole onto Fe(1 0 0) surface. Electrochim Acta 112(1):577–586

26. Ebenso EE, Kabanda MM, Arslan T, Saracoglu M, Kandemirli F, Murulana LC, Singh AK, Shukla SK, Hammouti B, Khaled KF, Quraishi MA, Obot IB, Eddy NO (2012) Quantum chemical investigations on quinoline derivatives as effective corrosion inhibitors for mild steel in acidic medium. Int J Electrochem Sci 7:5643–5676

27. Kabanda MM, Murulana LC, Ebenso EE (2012) Theoretical studies on phenazine and related compounds as corrosion inhibitors for mild steel in sulphuric acid medium. Int J Electrochem Sci 7:7179–7205

28. Kabanda MM, Ebenso EE (2012) Density functional theory and quantitative structure–activity relationship studies of some quinoxaline derivatives as potential corrosion inhibitors for copper in acidic medium. Int J Electrochem Sci 7:8713–8733

29. Caliskan N, Akbas E (2012) Corrosion inhibition of austenitic stainless steel by some pyrimidine compounds in hydrochloric acid. Mater Corros 3:231–237

30. Frisch MJ, Trucks GW, Schlegel HB, Scuseria GE, Robb MA, Cheeseman JR, Scalmani G, Barone V, Mennucci B, Petersson GA, Nakatsuji H, Caricato M, Li X, Hratchian HP, Izmaylov AF, Bloino J, Zheng G, Sonnenberg JL, Hada M, Ehara M, Toyota K, Fukuda R, Hasegawa J, Ishida M, Nakajima T, Honda Y, Kitao O, Nakai H, Vreven T, Montgomery JA, Jr, Peralta JE, Ogliaro F, Bearpark M, Heyd JJ, Brothers E, Kudin KN, Staroverov VN, Keith T, Kobayashi R, Normand J, Raghavachari K, Rendell A, Burant JC, Iyengar SS, Tomasi J, Cossi M, Rega N, Millam JM, Klene M, Knox JE, Cross JB, Bakken V, Adamo C, Jaramillo J, Gomperts R, Stratmann RE, Yazyev O, Austin AJ, Cammi R, Pomelli C, Ochterski JW, Martin RL, Morokuma K, Zakrzewski VG, Voth GA, Salvador P, Dannenberg JJ, Dapprich S, Daniels AD, Farkas O, Foresman JB, Ortiz JV, Cioslowski J, Fox DJ (2010) Gaussian, Inc., Wallingford

31. Li W, Zhao X, Liu F, Deng J, Hou B (2009) Investigation on the corrosion inhibitive effect of 2H-pyrazole-triazole derivatives in acidic solution. Mater Corros 60:287–293

32. Hasanov R, Sadikoglu M, Bilgic S (2007) Electrochemical and quantum chemical studies of some Schiff bases on the corrosion of steel in H_2SO_4 solution. Appl Surf Sci 253:3913–3921

33. Pearson RG (1988) Chemical hardness and bond dissociation energies. J Am Chem Soc 110:7684–7690

34. Masoud MS, Awad KM, Shaker MA, El-Tahawy MMT (2010) The role of structural chemistry in the inhibitive performance of some aminopyrimidines on the corrosion of steel. Corros Sci 52:2387–2396

35. Zhan CG, Nichols JA, Dixon DA (2003) Ionization potential, electron affinity, electronegativity, hardness, and electron excitation energy: molecular properties from density functional theory orbital energies. J Phys Chem A 107:4184–4195

36. Parr RG, Pearson RG (1983) Absolute hardness: companion parameter to absolute electronegativity. J Am Chem Soc 105:7512–7516

37. Yang W, Parr RG (1985) Hardness, softness, and the Fukui function in the electronic theory of metals and catalysis. Proc Natl Acad Sci 82:6723–6726

38. Parr RG, Szentpaly LV, Liu S (1999) Electrophilicity index. J Am Chem Soc 121:1922–1924

39. Gázquez JL, Cedillo A, Vela A (2007) Electrodonating and electroaccepting powers. J Phys Chem A 111:1966–1970

40. Chattaraj PK, Giri S, Duley S (2011) Update 2 of: electrophilicity index. Chem Rev 111:PR43–PR75

41. Gómez B, Likhanova NV, Domínguez-Aguilar MA, Martínez-Palou R, Vela A, Gázquez JL (2006) Quantum chemical study of the inhibitive properties of 2-pyridyl-azoles. J Phys Chem B 110:8928–8934

42. Lece HD, Emregül KC, Atakol O (2008) Difference in the inhibitive effect of some Schiff base compounds containing oxygen, nitrogen and sulfur donors. Corros Sci 50:1460–1468

43. Nataraja SE, Venkatesha TV, Tandon TV, Shylesha BS (2011) Quantum chemical and experimental characterization of the effect of ziprasidone on the corrosion inhibition of steel in acid media. Corros Sci 53:41094117

44. Li X, Deng S, Fu H, Li T (2009) Adsorption and inhibition effect of 6-benzylaminopurine on cold rolled steel in 1.0 M HCl. Electrochim Acta 54:4089–4098

45. Cancès E, Mennucic B, Tomasi J (1997) A new integral equation formalism for the polarizable continuum model: theoretical background and applications to isotropic and anisotropic dielectrics. J Chem Phys 107:3032–3041

46. El-Ashry ES, Senior SA (2011) QSAR of lauric hydrazide and its salts as corrosion inhibitors by using the quantum chemical and topological descriptors. Corros Sci 53:1025–1034

47. Chattaraj PK, Chakraborty A, Giri S (2009) Net electrophilicity. J Phys Chem A 113:10068–10071

48. Sastri VS, Perumareddi JR (1997) Molecular orbital theoretical studies of some organic corrosion inhibitors. Corrosion 53:617–622

49. Musa AY, Kadhum AAH, Mohamad AB, Rahoma AAB, Mesmari H (2010) Electrochemical and quantum chemical calculations on 4,4-dimethyloxazolidine-2-thione as inhibitor for mild steel corrosion in hydrochloric acid. J Mol Struct 969:233–237

50. Weiler-Feilchenfeld H, Pullman A, Berthod H, Giessner-Prettre C (1970) Experimental and quantum-chemical studies of the dipole moments of quinoline and indole. J Mol Struct 6:297–304

51. Jensen F (1999) Introduction to computational chemistry. Wiley, Chichester

52. Gece G, Bilgic S (2010) A theoretical study on the inhibition efficiencies of some amino acids as corrosion inhibitors of nickel. Corros Sci 52:3435–3443

53. Yang Y, Mortier WJ (1986) The use of global and local molecular parameters for the analysis of the gas-phase basicity of amines. J Am Chem Soc 108:5708–5711

54. Al-Mobarak NA, Khaled KF, Hamed MNH, Abdel-Azim KM, Abdelshafi NS (2010) Corrosion inhibition of copper in chloride media by 2-mercapto-4-(p-methoxyphenyl)-6-oxo-1,6-dihydropyrimidine-5-carbonitrile: electrochemical and theoretical study. Arab J Chem 3:233–242

55. Musa AY, Khadom AA, Kadhum AAH, Mohamad AB, Takriff MS (2010) Experimental and theoretical study on the inhibition performance of triazole compounds for mild steel corrosion. Corros Sci 52:3331–3340